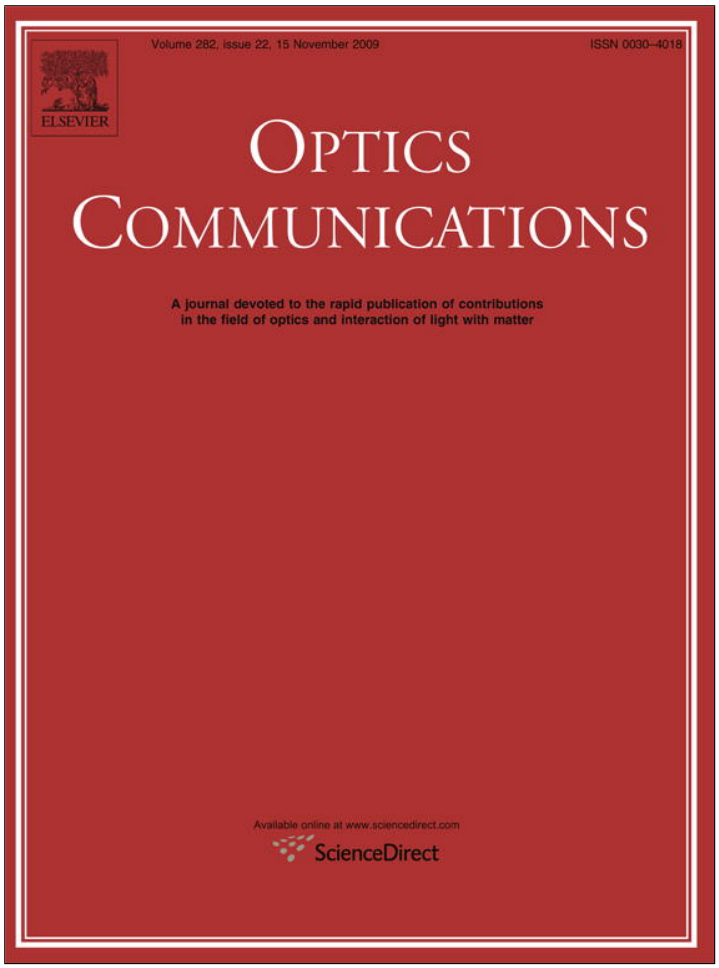

Optics Communications 282 (2009) 4418–4422

Contents lists available at ScienceDirect

Optics Communications

journal homepage: www.elsevier.com/locate/optcom

Simulation of turbulence in mode-locked lasers

G.H.C. New *, M. Noy, J.A. Crosse, A. Rumley, L. Newson, Z.-Y. Chen, C. Cheung, A. Todhunter

The Blackett Laboratory, Imperial College London, London SW7 2AZ, UK

ARTICLE INFO

Article history:
Received 30 May 2009
Received in revised form 5 August 2009
Accepted 5 August 2009

PACS:
42.60.Fc
42.60.Mi
42.65.Re
47.27.Cn

Keywords:
Mode-locking
Dynamical laser instabilities
Transition to turbulence
Optical pulse generation

ABSTRACT

We establish the connection between a paper by Kartner et al. [F.X. Kartner, D.M. Zumbuhl, N. Matuschek, Phys. Rev. Lett. 82 (1999) 4428] entitled "Turbulence in mode-locked lasers", and earlier work on the role of noise in mode-locked laser systems. We present numerical results that broadly support the analytical results of Kartner et al.

1. Introduction

In 1999, Kartner et al. [1] examined the relationship between fluid turbulence and the dynamics of actively mode-locked (AML) lasers detuned from resonance. These authors derived a normalised detuning parameter that (they argued) plays the same role in AML lasers as Reynolds' number in hydrodynamics. In the present paper, we highlight the link between the phenomenon investigated in [1], and earlier work on noise-induced fluctuations in lasers and laser amplifiers. In addition, we present the results of numerical simulations that broadly support the analytical results of Kartner et al.

In 1979, Hopf and Overman [2] showed that an optical pulse propagating in a nonlinear swept-gain amplifier (NLSGA) is highly sensitive to random perturbations originating in the background noise far out on its leading edge. Since the pulse envelope in an NLSGA travels faster than the noise background, it overtakes the noise, picking up stochastic features in the process. These move progressively up the leading edge, over the peak, and down the trailing edge to be lost in the noise to the rear. Although the noise itself is weak, the perturbations to the pulse profiles can be severe. The fluctuations (especially phase fluctuations) in the noise seriously disturb the integrity of the pulse, and strong macroscopic disturbances in pulse shape and energy are created.

Effects of this kind are not confined to swept-gain amplifiers, but occur equally in actively mode-locked lasers when these are detuned from resonance. Detuning forces the mode-locked pulse envelope to travel at a different speed to the fluctuations in noise surrounding it. If the drive frequency is raised, the pulse is forced forward into the noise in front of it (as in the NLSGA); if the frequency is lowered, the pulse is forced backwards into the noise behind it. In both cases, the pulse becomes subject to the same kind of perturbations that occur in an NLSGA. The problem was especially serious when synchronously mode-locked dye lasers were in common use for short pulse generation in the 1980s and 1990s. In synchronous mode-locking, optimal pulse shapes occur when the pump frequency is slightly higher than perfect resonance [3], so the pulses were vulnerable to noise encroachment on the leading edge. However, the self-seeding technique discovered by Beaud et al. [4] proved highly effective in protecting the pulses from the noise around them [5–8], and was used very successfully for stabilising laboratory systems [9].

The present paper is organised as follows. In Section 2, the actively mode-locked laser model used for the simulations is described. This provides a convenient context for introducing the parameters governing the behaviour of the laser and for making connections with earlier work. Particular attention is given to the properties of the Fabry–Perot filter. The normalised detuning

* Corresponding author. Tel.: +44 20 7594 7791; fax: +44 20 7594 7714.
E-mail address: g.new@imperial.ac.uk (G.H.C. New).

0030-4018/$ - see front matter © 2009 Elsevier B.V. All rights reserved.
doi:10.1016/j.optcom.2009.08.007

parameter Δ introduced by Kartner et al. in [1] is defined and we explain how, according to [1], the behaviour of a laser is predicted to depend on the value of Δ. The formula for the steady-state pulse width near perfect detuning is stated and explained.

In Section 3, we present a range of simulations illustrating the physical phenomenon that destabilises mode-locked lasers detuned from resonance, and results are presented that are in good agreement with the predictions of [1].

2. Laser model

2.1. Gain, loss and modulation

The actively mode-locked laser model is based on a ring cavity in which the electric field E is defined at N uniformly-spaced points separated by δz in space or $\delta t = \delta z/c$ in time. The nominal round-trip time is therefore $T_{cav} = N\delta t$. The ring contains a modulator, a gain medium, and a bandwidth-limiting filter. The field transmission factor of the modulator is

$$m(t) = \exp\left\{-\frac{1}{2}M(t)\right\} \tag{1}$$

where $M(t) = D(1-\cos\omega_m t)$, D is the modulation depth, and the period of the modulator $T_{mod} = 2\pi/\omega_m$. The corresponding field transmission factor of the laser material is

$$g(t) = \exp\left\{\frac{1}{2}(A(t) - \Gamma)\right\} \tag{2}$$

The time-dependent amplification coefficient $A(t)$ is governed by the differential equation.

$$\frac{dA}{dt} = \frac{A_u - A}{T_1} - A\sigma F \tag{3}$$

where A_u is the unsaturated (small signal) value of A, T_1 is the population relaxation time, σ is the transition cross-section, and F is the photon flux. The parameter Γ in Eq. (2) represents losses of all origins. Note that the equilibrium solution of Eq. (3) is

$$A = \frac{A_u}{1 + \sigma T_1 F} \tag{4}$$

The factors of $\frac{1}{2}$ in Eqs. (1) and (2) appear because $m(t)$ and $g(t)$ are the transmission factors for the *field*, whereas the coefficients D, A, and Γ relate to the *intensity* (or photon flux).

We used a Fabry–Perot Etalon (FPE) as the bandwidth-limiting filter since it can be implemented in the time domain simply and without approximation; a thorough discussion is given in Section 2.2. A stochastic noise source was included to simulate spontaneous emission; full details can be found in [11], and references therein.

2.2. Fabry–Perot Etalon

The Fabry–Perot Etalon (FPE) consists of a pair of identical partially-reflecting plates separated by a spacing s. The device has peak transmission at a set of equally-spaced resonance frequencies $\nu_q = q\delta\nu_{FSR} = q/t_e$, where q is an integer, and the frequency separation $\delta\nu_{FSR}$ (the *free spectral range*) is the inverse of the etalon transit time $t_e = 2s/c$. The field reflection factor of the plates is r, and the corresponding transmission factor is t (not to be confused with time). The *intensity* reflection and transmission factors are respectively $R = r^2$ and $T = t^2$, where $R + T = 1$ ensures conservation of energy.

The characteristic time of the filter t_f is conveniently defined as the impulse response time of the FPE in the equation.

$$R = \exp\{-t_e/t_f\} \tag{5}$$

so $t_f = -t_e \ln R$. If we equate t_e with the unit of time in the field mesh δt, it is easy to show that the input/output relationship of the filter is [3,5]

$$E_j^{out} = T\sum_{k=-\infty}^{j} R^{j-k}E_k^{in} = TE_j^{in} + RE_{j-1}^{out} \tag{6}$$

The equation is generally applicable for a time-varying complex field exhibiting amplitude and phase fluctuations. For a monochromatic input field, Eq. (6) gives the filter transmission factor as

$$f = \frac{E_j^{out}}{E_j^{in}} = |f|e^{i\phi} = T(1 + S + S^2 + \ldots + S^n + \ldots) = \frac{T}{(1-S)} \tag{7}$$

where ϕ is the argument of f, $S = R\exp\{-i\delta\}$, $\delta = (\omega - \omega_0)t_e$, and ω_0 is an etalon resonance frequency.

Eq. (7) allows two important properties of the FPE to be calculated. The first is the group time delay of the filter which is given by

$$t_d = -\left.\frac{d\phi}{d\omega}\right|_{\delta=0} = \frac{t_e R}{T} \approx t_f - \frac{1}{2}t_e \tag{8}$$

As shown in Section 3, the delay affects the accurate tuning of the modulator. The other key property of the FPE is the second derivative of $|f|$ namely

$$\left.\frac{d^2|f|}{d\omega^2}\right|_{\delta=0} = -\frac{t_e^2 R}{T^2} \cong -\left(t_f^2 - \frac{1}{4}t_e^2\right) \tag{9}$$

This is a measure of the bandwidth-limiting properties of the filter which, in turn, determines the mode-locked pulse duration in the steady-state. When $t_f \gg t_e$, the second term in the final bracket of Eq. (9) can be ignored.

2.3. Modulator detuning and the normalised detuning parameter

A crucial parameter determining the performance of the laser is the modulator detuning defined as the difference between the cavity transit time and the modulator period namely $t_m = T_{cav} - T_{mod}$. However, as we saw in B above, the FPE introduces a delay t_d, so the effective cavity transit time is increased to $T'_{cav} = T_{cav} + t_d$, and the corresponding effective detuning is $t'_m = T'_{cav} - T_{mod}$. We can expect the laser to deliver optimal performance near $t'_m = 0$, and we will refer to this as "exact" or "perfect" tuning.

Kartner et al. [1] introduced a normalised detuning parameter Δ which they argued plays a role similar to that of Reynolds' number in fluid dynamics. The definition was

$$\Delta = \frac{1}{2\sqrt{2D_f M_s}}\frac{T_d}{T_a} = -\frac{t'_m}{t_f}\sqrt{\frac{T_{mod}}{2\pi\sqrt{2D}\,t_f}} \tag{10}$$

where the second step expresses the result in terms of parameters defined in this paper using the links $D_f = \frac{1}{2}t_f^2$, $M_s = \pi^2 D/T_{mod}^2$, $T_a = \sqrt[4]{D_f/M_s}$ and $T_d = -t'_m$.

In [1], it was shown that the transient gain on the wings of the pulses scales as $\exp\{2\Delta^2\}$, that an actively mode-locked laser is already highly sensitive to perturbations for $|\Delta| \sim 3$, and that the transition to turbulence occurs near $|\Delta| = 3.7$. However, the authors noted that the critical detuning falls to $|\Delta| \sim 2$ in the presence of spontaneous emission noise, a value that is weakly dependent on the strength of the noise.

2.4. Pulse width near perfect tuning

Close to perfect tuning, the steady-state pulse width Δt of the actively mode-locked laser can be estimated from the equation.

$$\left(1 - \frac{D\pi^2\Delta t^2}{4\ln 2\, T_{mod}^2}\right)\left(1 + \frac{2\ln 2\, t_f^2}{\Delta t^2}\right) = 1 \tag{11}$$

where the brackets represent respectively the pulse narrowing factor from a pass through the modulator (which involves Eq. (1)), and the pulse broadening factor from a pass through the filter (which involves Eq. (9)). We note that the second term on the right-hand side of Eq. (9) has been ignored in Eq. (11).

It follows from Eq. (11) that [10].

$$\frac{\Delta t}{T_{cav}} \approx \sqrt{\left(\sqrt{\frac{2}{D}}\frac{2\ln 2}{\pi}\frac{t_f}{T_{cav}}\right)} \tag{12}$$

As will be demonstrated in the Section 3, numerical simulations based on the laser model described are in good agreement with this equation.

3. Simulations

3.1. Parameter values

The basic parameter set used for the simulations was $A = 0.5$, $\Gamma = 0.2$, $D = 0.2$, and $R = 0.8$. It follows that $T = 1 - R = 0.2$, the filter delay time $t_d = t_e R/T = 4t_e$ (from Eq. (8)), and the characteristic time $t_f = -t_e \ln R = 4.48t_e$ (from Eq. (5)). We divide the cavity into $N = 1024$ equally-spaced mesh points and, since we have chosen to identify the mesh time unit δt with t_e, the parameters t_d and t_f correspond to 4 and 4.48 mesh units, respectively. Since the modulator period T_{mod} is close to T_{cav}, Eq. (10) yields $\Delta = -7.58\ (t'_m/t_f)$.

An important factor determining the overall dynamic properties of the laser is the characteristic time T_1 in Eq. (2). It is of course well-known that strong Q-switching requires high values of T_1, whereas Q-switching will certainly be weak when $T_1 \sim T_{cav}$, and may not be achievable at all. The pulse profiles will also be strongly influenced by gain saturation in the latter case. Given that we are principally interested in CW mode-locking in this paper, setting T_1 too high means that the laser takes a long time (typically T_1/T_{cav} transits) to settle down; indeed, for large modulator detuning, limit cycle behaviour can sometimes occur where no equilibrium state is ever reached. Fortunately, it turns out that the value of T_1 is largely irrelevant to the central issue of this paper, and so we choose $T_1 = 50T_{cav}$, which is high enough to limit the influence of gain saturation, but not so high that Q-switching instabilities are encountered. We note that T_1/T_{cav} is in the range $10^4 - 10^6$ in typical solid-state lasers!

The level and type of noise injection are also significant issues. Close to perfect modulator tuning, unperturbed steady-state mode-locking is achieved whether noise is injected or not. However, when the detuning is increased to beyond about $|\Delta| = 2$, noise starts to play a role, the more so as the detuning is increased further. Depending on the precise parameter values, the laser might switch off altogether in the absence of noise, but exhibit steady-state mode locking if a weak coherent (i.e. non-stochastic) signal were injected. On the other hand, in the presence of *stochastic* background noise, it will exhibit the macroscopic perturbations that are the focus of attention in this paper.

3.2. Results and discussion

Fig. 1 shows the mode-locked pulse profile (plotted on a log scale against the left-hand axis) for the case of nominally perfect tuning ($t'_m = 0$). Notice that the wings of the pulse are embedded in a sea of noise. However, for this tuning condition, the pulse is not disturbed by the noise, any more than a rocky outcrop in the ocean is disturbed by the waves that break upon it. The abscissa time scale is in units of T_{cav}, with maximum modulator transmission at the centre of the frame (=0.5) and minimum transmission

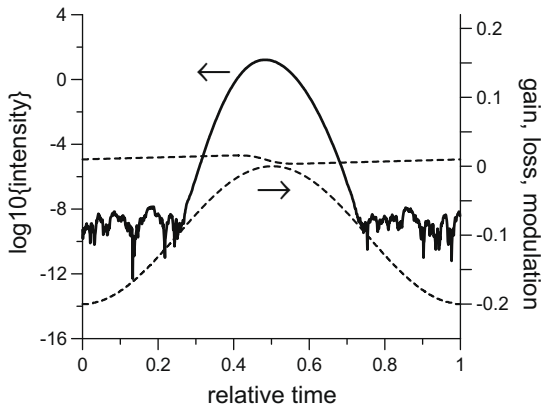

Fig. 1. Steady-state pulse profile at nominally perfect tuning (solid line) plotted on the left-hand $\log_{10}$ intensity scale. The parameter values are detailed in Section 3.1. The upper and lower dotted lines show the respective variations of $A(t) - \Gamma$ and $M(t)$ (against the right-hand axis).

at the extremities (=0 and 1). The upper and lower dotted lines (plotted against the right-hand axis) show the respective time variations of the gain (represented by $A(t) - \Gamma$; see Eqs. (2)–(4)), and the modulation $-M(t)$ (Eq. (1)). Careful inspection of the figure reveals the slight depletion in the gain caused by the passage of the pulse, and the subsequent gain recovery. This effect becomes more pronounced if T_1/T_{cav} is reduced from the value of 50 used for the figure, but progressively disappears as the value is raised. The pulse full width at half maximum intensity is $0.0793T_{cav}$,which is close to the value of $0.0781T_{cav}$ predicted by Eq. (11).

The effect of detuning on the steady-state pulse width is shown in Fig. 2. The thick line, plotted against the left-hand axis shows the pulse width (expressed as a fraction of T_{cav}) as a function of t'_m/t_f. As noted already, for small detuning, steady-state operation is achieved irrespective of background noise, and the line is shown as solid in this region. For larger detuning, stochastic background noise normally prevents the realisation of steady-state operation, and so coherent signal injection was used to create artificial steady-state pulse profiles whose widths are plotted as a dotted line. The pulse width predicted by Eq. (11), which can be expected to apply near perfect tuning, is shown as a circular dot. The shape

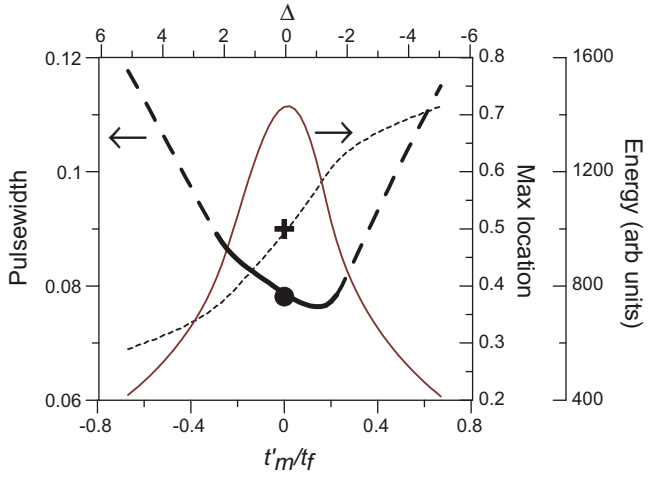

Fig. 2. Steady-state pulse width variation as a function of detuning (solid curve) plotted against the left-hand scale. The dotted line (plotted against the first right-hand scale) shows the variation of position of the pulse within the modulation cycle. The bell-shaped solid curve (against the second right-hand scale) shows the corresponding variation in pulse energy.

of the curve (particularly the skewing near $t'_m = 0$) parallels the analytical result plotted in Fig. 3 of [10].

The thin dotted line in Fig. 2 (plotted against the first right-hand axis) shows how the position of the mode-locked pulse changes within the modulation cycle as the modulator tuning is varied. As we have seen already, for $t'_m = 0$ the pulse is positioned near the peak of the modulator; however, it arrives ahead of the peak for shorter cavities, and behind the peak when the cavity is lengthened. The curve tends to 0.25 and 0.75 in the respective limits; the position (0.5, 0.5) is marked with a cross.

The bell-shaped thin line in the figure (plotted against the second right-hand axis) traces the variation in the pulse energy, which drops as the detuning is increased. This behaviour is to be expected given that, under detuned conditions, the pulse no longer passes through the modulator at the point of maximum transmission.

The detuning range in Fig. 2 is $t'_m/t_f = \pm 0.8$, which corresponds to $\Delta = \mp 6.06$; hence, for the larger detunings in the figure, the system can be expected to exhibit turbulence. Fig. 3 shows what happens for $\Delta = -2.0$. The lower curve (plotted against the left-hand axis) shows the variation in the peak intensity of the mode-locked pulse over 5000 transits. Instead of settling down to a flat line, the graph shows that the pulse experiences a random sequence of perturbations, each of which is accompanied by a wobble in the position of the pulse within the modulator cycle, shown in the upper graph (against the RH axis). The anatomy of these events has been examined in detail elsewhere (see e.g. [3,5,7,8,11]). In each case, a fluctuation originating in the sea of noise ahead of the pulse moves progressively through the profile. As it moves up the leading edge and approaches the pulse centre, a new peak emerges in front of the existing peak, which in time usurps its partner, which then retreats down the trailing edge to be lost in the noise to the rear. The sudden rise in the pulse width in the middle of each event (lower trace) occurs at the moment when the full width at half maximum intensity embraces a twin-peaked profile, while the corresponding downward jump in the upper trace marks the point when the new peak rises above the old one.

It is interesting to compare Fig. 3 with Fig. 4 where $\Delta = +2.88$. With the change of sign, the movement of noise perturbations across the pulse profile is now from back to front. Compare the upper traces in two figures; in Fig. 3, the movement of the peak is normally from front to back (from lower to higher relative positions), whereas in Fig. 4, the direction is reversed. The higher magnitude of Δ in Fig. 4 also means that the event frequency is increased.

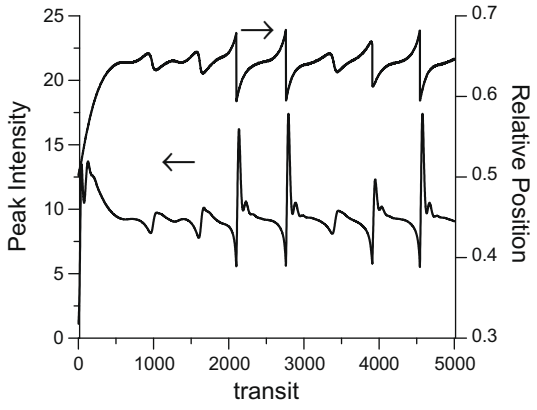

Fig. 3. Peak intensity fluctuations for a detuned laser with $\Delta = -2$ in the presence of stochastic background noise (lower curve, left-hand axis). The corresponding variation in the peak position of the pulse is traced in the upper curve (right-hand axis).

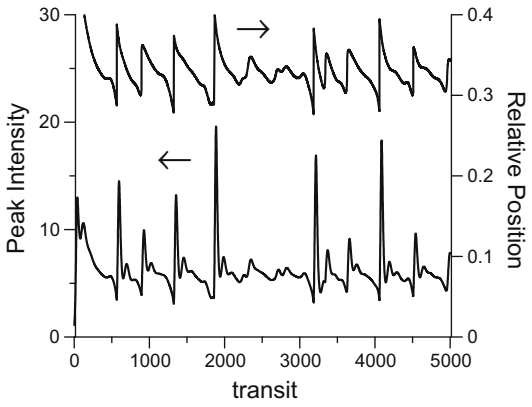

Fig. 4. As Fig. 3, but at $\Delta = +2.88$.

To verify the proposition of Kartner et al. [1] that a transition to turbulence occurs in the vicinity of $|\Delta| \sim 2$, it was necessary to devise a numerical measure of perturbation. The procedure adopted was based on the behaviour of the peak intensity in Figs. 3 and 4. In the interval between 1500 and 5000 transits (after the initial transient has died away), we recorded the fraction of transits in which the peak intensity differed from the mean value by more than 2%. This number, averaged over 1000 different random noise sequences and termed the perturbation factor, is plotted in Fig. 5 as a function of Δ for three different values of the injected noise intensity. The bold line (for a noise intensity of 10^{-10}) indicates that in the range $-1.8 < \Delta < 2.2$ the perturbation factor is zero and the system is stable. However, for even a slight increase in the magnitude of Δ on either side of the stable region, the factor rises very rapidly towards 1.

The graph in Fig. 5 is largely insensitive to the value of T_1, and only weakly dependent on the injected noise intensity. Lowering the noise widens the region of stability, and vice versa, but the effect is relatively slight. The two thin lines in the figure are for noise intensities of 10^{-6} and 10^{-14}, four orders of magnitude above and below the value used for the bold line. Changing the coherence time of the noise also has very little effect. The 2% figure used to calculate the instability factor is of course arbitrary. But raising the percentage to 5% or 10%, while admittedly making the walls on either side somewhat less precipitous, has little effect on the width of the stability region.

The slight asymmetry in Fig. 5 requires comment. A remote possibility is that the apparent rightward shift of about 0.2 in Δ results from a discrepancy in the formula $T'_{cav} = T_{cav} + t_d$ for the effective

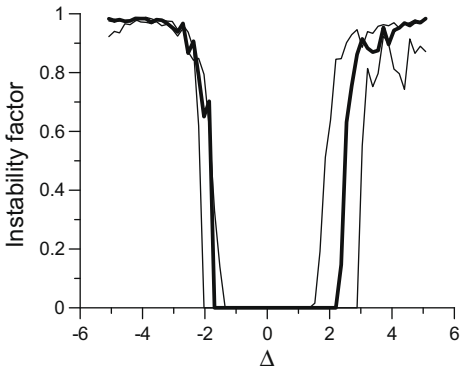

Fig. 5. The instability factor as a function of Δ. The bold line is for a noise level of 10^{-10}, while the inner and outer thin lines are for respective noise levels of 10^{-6} and 10^{-14}.

cavity transit time. An increase of just 3% in t_d would shift the curves in Fig. 5 leftwards by 0.2. However, close inspection of the figure shows that the stability boundary is more sensitive to the noise intensity for positive Δ than for negative Δ; indeed the low noise line in the figure shows a much greater displacement than the high noise line. We therefore conjecture that the shift may have another cause. Two different physical processes govern the flow of information across the mode-locked pulse. One is the detuning of the modulator, which can be of either sign. The other arises in the filter, and this can only result in delay. It follows that when Δ is negative ($t'_m > 0$), both flows are from front to back whereas, when Δ is positive ($t'_m < 0$), the two flows are in opposition. We suggest that this fundamental detuning asymmetry may be responsible for the effects seen in Fig. 5.

4. Conclusion

In conclusion, we have pointed out the connection between the work of Kartner et al. [1] and earlier work on the role of noise in mode-locked lasers and laser amplifiers. We have also presented numerical results that generally confirm the analytical formulae obtained in [1]. In particular, the transition to turbulence in a detuned actively mode-locked laser has been shown to be sharp, and to occur near $|\Delta| = 2$ in the presence of a stochastic noise background; the width of the region of stability has been found to depend on the noise level, albeit only weakly. These results are consistent with the predictions made in [1].

As noted in the introduction, the phenomena discussed in this paper were originally identified in swept-gain laser amplifiers [2], and were studied in detail in the context of synchronously mode-locked dye lasers [3–9]. Dye lasers themselves are of course rarely used today, but it is important to recognise that the potential for noise-induced jitter is a general feature of synchronously-pumped devices. As far as lasers are concerned, synchronous mode-locking is still employed in Cr:YAG and Cr:ZnSe systems. On the other hand, synchronously-pumped optical parametric oscillators (SPOPOs) are now in widespread use, and noise-induced jitter is an issue there too. SPOPOs exhibit more complicated dynamics than their laser counterparts because three interacting pulses (pump, signal, and idler) are involved rather than two, and because the signal is usually free to shift its wavelength to bring its group velocity into synchronism with the pump. A detailed analysis of noise in the SPOPO case can be found in [12].

Acknowledgements

Useful conversations with Professor Derryck Reid (Heriot-Watt University) and Professor Roy Taylor (Imperial College) are gratefully acknowledged. Seven of the authors worked on this topic for their undergraduate projects at Imperial College at various times between 2001 and 2008. The eighth author (GHCN) is grateful to the Leverhulme Trust for the award of an Emeritus Fellowship, which has finally provided the opportunity for this work to be written up.

References

[1] F.X. Kartner, D.M. Zumbuhl, N. Matuschek, Phys. Rev. Lett. 82 (1999) 4428.
[2] F.A. Hopf, M.A. Overman, Phys. Rev. A 19 (1979) 1180.
[3] J.M. Catherall, G.H.C. New, IEEE J. Quantum Electron. QE-22 (1986) 1593.
[4] P. Beaud, J.Q. Bi, W. Hodel, H.P. Weber, Opt. Commun. 80 (1990) 31.
[5] G.H.C. New, Opt. Lett. 15 (1990) 1306.
[6] J.Q. Bi, W. Hodel, H.P. Weber, Opt. Commun. 81 (1991) 408.
[7] W. Forysiak, J.V. Moloney, Phys. Rev. A 45 (1992) 3275.
[8] W. Forysiak, J.V. Moloney, Phys. Rev. A 45 (1992) 8110.
[9] C.J. Hooker, J.M.D. Lister, I.N. Ross, Opt. Commun. 80 (1991) 375.
[10] G.H.C. New, L.A. Zenteno, P.M. Radmore, Opt. Commun. 48 (1983) 149.
[11] G.H.C. New, D. Wood, J. Mod. Opt. 38 (1991) 785.
[12] A.J. Scroggie, G.-L. Oppo, G. Alessandro, J. Opt. Soc. Am. B 17 (2000) 84.